New Journal of Physics
An Institute of Physics and Deutsche Physikalische Gesellschaft Journal

Dissipation caused by a vorticity field and generation of singularities in Madelung fluid

M Caliari[1], **G Inverso**[2] **and L M Morato**[1,3]

[1] Faculty of Mathematical, Physical and Natural Science, University of Verona, Italy
[2] Elvis Elettronica, Padova, Italy
E-mail: morato@sci.univr.it

New Journal of Physics **6** (2004) 69
Received 6 April 2004
Published 5 July 2004
Online at http://www.njp.org/
doi:10.1088/1367-2630/6/1/069

Abstract. We consider a generalization of Madelung fluid equations, which was derived in the 1980s by means of a pathwise stochastic calculus of variations with the classical action functional. At variance with the original ones, the new equations allow us to consider velocity fields with vorticity. Such a vorticity causes dissipation of energy and it may concentrate, asymptotically, in the zeros of the density of the fluid. We study, by means of numerical methods, some Cauchy problems for the bidimensional symmetric harmonic oscillator and observe the generation of zeros of the density and concentration of the vorticity close to central lines and cylindrical sheets. Moreover, keeping the same initial data, we perturb the harmonic potential by a term proportional to the density of the fluid, thus obtaining an extension with vorticity of the Gross–Pitaevskii equation, and observe analogous behaviours.

[3] Corresponding author: Department of Computer Science, Ca' Vignal 2-strada Le Grazie 15, 37134 Verona, Italy.

PII: S1367-2630(04)79056-4

Contents

1. Introduction

In this paper we study, by means of numerical methods, some Cauchy problems for a dissipative generalization of Madelung fluid equations. Such a generalization was introduced in [1]–[3] as a solution of a stochastic variational problem for the classical action functional, in the framework of Nelson stochastic quantization (see [4]–[8] for general mathematical and physical aspects). For a spin-less particle of mass m subjected to a scalar potential $\tilde{\Phi}(\tilde{\boldsymbol{x}})$, denoting by $\tilde{\rho}(\tilde{\boldsymbol{x}}, \tilde{t})$ the probability density and by $\tilde{\boldsymbol{v}}(\tilde{\boldsymbol{x}}, \tilde{t})$ the current velocity (the tilde sign is used for *dimensional* variables), the new equations read (omitting the independent variables)

$$\partial_{\tilde{t}}\tilde{\boldsymbol{v}} + (\tilde{\boldsymbol{v}}\cdot\tilde{\nabla})\tilde{\boldsymbol{v}} - \frac{\hbar^2}{2m^2}\tilde{\nabla}\left(\frac{\tilde{\nabla}^2\sqrt{\tilde{\rho}}}{\sqrt{\tilde{\rho}}}\right) + \frac{\hbar}{2m}(\tilde{\nabla}\ln\tilde{\rho} + \tilde{\nabla})\wedge(\tilde{\nabla}\wedge\tilde{\boldsymbol{v}}) = -\frac{1}{m}\tilde{\nabla}\tilde{\Phi},$$

$$\partial_{\tilde{t}}\tilde{\rho} = -\tilde{\nabla}\cdot(\tilde{\rho}\tilde{\boldsymbol{v}}). \tag{1}$$

(A generalization to curved spaces is given in [9]. A version where the rotational term is multiplied by a positive constant playing the role of a free parameter is proposed in [10].) Now let $\tilde{Q}$ denote an open subset of $\mathbb{R}^3$. If $\tilde{\rho}$ is strictly positive and $\tilde{\nabla}\wedge\tilde{\boldsymbol{v}}$ is equal to zero on $\tilde{Q}$ for all $\tilde{t}$, then, by Madelung transformations

$$\tilde{\boldsymbol{v}}(\tilde{\boldsymbol{x}}, \tilde{t}) = \frac{1}{m}\tilde{\nabla}\tilde{S}(\tilde{\boldsymbol{x}}, \tilde{t}), \quad \tilde{\boldsymbol{x}} \in \tilde{Q},$$

$$\tilde{\rho}(\tilde{\boldsymbol{x}}, \tilde{t})^{1/2}\exp\left[\mathrm{i}\frac{\tilde{S}(\tilde{\boldsymbol{x}}, \tilde{t})}{\hbar}\right] = \tilde{\psi}(\tilde{\boldsymbol{x}}, \tilde{t}), \quad \tilde{\boldsymbol{x}} \in \tilde{Q},$$

system (1) turns to be equivalent to the Schrödinger equation

$$\mathrm{i}\hbar\partial_{\tilde{t}}\tilde{\psi} = -\frac{\hbar^2}{2m}\tilde{\nabla}^2\tilde{\psi} + \tilde{\Phi}\tilde{\psi}, \tag{2}$$

where $\tilde{\psi}$ has domain $\tilde{Q}$ for all $\tilde{t}$.

Coming back to the original equations (1) on $\mathbb{R}^3$ we can define, for any sufficiently smooth solution $(\tilde{\rho}, \tilde{\boldsymbol{v}})$, $\tilde{\rho}$ being a probability density, the energy functional

$$\tilde{E}(\tilde{\rho}, \tilde{\boldsymbol{v}}) = \int_{\mathbb{R}^3} \left[\frac{1}{2} m(|\tilde{\boldsymbol{v}}(\tilde{\boldsymbol{x}}, \tilde{t})|^2 + |\tilde{\boldsymbol{u}}(\tilde{\boldsymbol{x}}, \tilde{t})|^2) + \tilde{\Phi}(\tilde{\boldsymbol{x}}) \right] \tilde{\rho}(\tilde{\boldsymbol{x}}, \tilde{t}) \, \mathrm{d}\tilde{\boldsymbol{x}}, \tag{3}$$

where

$$\tilde{\boldsymbol{u}}(\tilde{\boldsymbol{x}}, \tilde{t}) = \frac{\hbar}{2m} \tilde{\nabla} \ln \tilde{\rho}(\tilde{\boldsymbol{x}}, \tilde{t})$$

is the *osmotic velocity*. Then, as a consequence of the Energy Theorem proved in [3], we have, if $\tilde{\rho}$ has a good behaviour at infinity,

$$\frac{\mathrm{d}}{\mathrm{d}\tilde{t}} \tilde{E}(\tilde{\rho}, \tilde{\boldsymbol{v}}) = -\frac{\hbar}{2} \int_{\mathbb{R}^3} |\tilde{\nabla} \wedge \tilde{\boldsymbol{v}}(\tilde{\boldsymbol{x}}, \tilde{t})|^2 \tilde{\rho}(\tilde{\boldsymbol{x}}, \tilde{t}) \, \mathrm{d}\tilde{\boldsymbol{x}} \tag{4}$$

and it can be seen that the set of solutions of (1) such that $\tilde{\rho} \cdot (\tilde{\nabla} \wedge \tilde{\boldsymbol{v}}) = 0$ acts as an attracting set. In particular, if $\tilde{\rho} \cdot (\tilde{\nabla} \wedge \tilde{\boldsymbol{v}})$ is equal to zero on the whole $\mathbb{R}^3$, then functional (3) becomes the usual quantum conserved energy

$$\tilde{E}(\tilde{\rho}, \tilde{\boldsymbol{v}}) = \left\langle \tilde{\psi}, \left(-\frac{\hbar^2}{2m} \tilde{\nabla}^2 + \tilde{\Phi} \right) \tilde{\psi} \right\rangle,$$

where $\langle \cdot, \cdot \rangle$ denotes the scalar product in $L^2(\mathbb{R}^3, \mathrm{d}\tilde{\boldsymbol{x}})$.

Roughly, the (in general time-dependent) solutions of Schrödinger equation are expected to be related to 'dynamical equilibrium solutions of system (1)'. This fact is qualitatively represented in figure 1, where

(i) $\tilde{\Sigma}$ is the set of initial data $(\tilde{\rho}_0, \tilde{\boldsymbol{v}}_0)$ (not necessarily smooth);

(ii) solid lines represent time evolution (denoted by $(\tilde{\rho}_{\tilde{t}}, \tilde{\boldsymbol{v}}_{\tilde{t}})$) which corresponds, by Madelung transformations, to solutions of the Schrödinger equation (these, stationary or non-stationary, can be singular functions, typically in the presence of nodes of the wave function);

(iii) broken lines represent time evolution of (1) for *smooth rotational* initial data.

It is natural at this point to ask the following questions:

- Can the dissipative evolution described by system (1) asymptotically reproduce singular solutions of Madelung equations (either time-dependent or stationary) even if the initial data $(\tilde{\rho}_0, \tilde{\boldsymbol{v}}_0)$ are smooth fields on $\mathbb{R}^3$?
- Does the vorticity monotonically decrease at every point of $\mathbb{R}^3$?
- Can residual vorticity asymptotically remain concentrated in the zeros of the density?

The first and the third questions are strictly connected. Indeed, a typical example of solutions with a singularity are those related to the eigenfunctions of the angular momentum for a symmetric bidimensional harmonic oscillator. They correspond on $\tilde{Q} = \mathbb{R}^2 \backslash \{(0, 0)\}$ to stationary solutions of Madelung equations, with density going to zero while approaching the point $\{(0, 0)\}$ and,

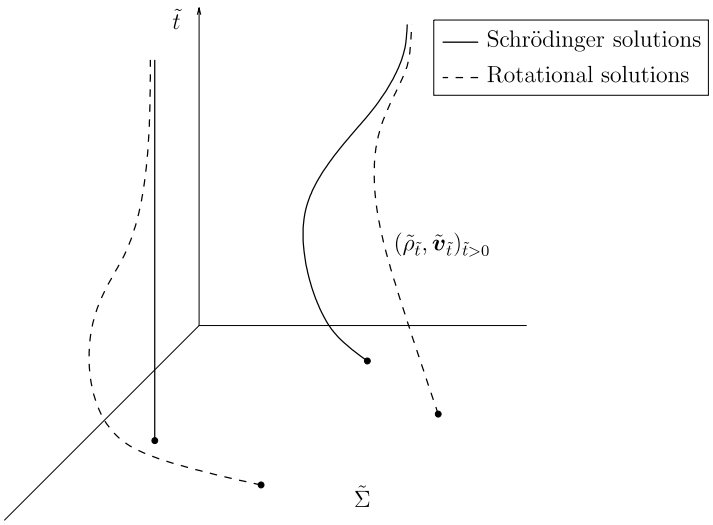

Figure 1. Schrödinger solutions as dynamical equilibrium states.

denoting by $(\tilde{r}, \theta)$ the polar coordinates on the plane, a velocity field defined by

$$\tilde{\boldsymbol{v}}(\tilde{r}) = \frac{\hbar}{m}\tilde{\nabla}(\ell\theta) = \frac{\hbar\ell}{m\tilde{r}}\hat{\theta}, \qquad \ell = 0, \pm 1, \pm 2, \ldots$$

which tends to infinity for $\tilde{r}$ approaching zero. The velocity field is irrotational on $\tilde{Q} = \mathbb{R}^2\backslash\{(0,0)\}$. The circulation for any closed path around $\{(0,0)\}$ is equal to $\ell\hbar/m$. In fact, all eigenfunctions of the angular momentum correspond to stationary solutions of Madelung equations, characterized by a quantized central vortex line (thinking of the system as being described in $\mathbb{R}^3$, the forces along the z-axis being equal to zero).

In this work we give some answers to the above-mentioned questions, by solving numerically the system of PDEs (1). In particular, we consider as initial data a linear velocity field with constant vorticity (which corresponds to that of a body rotation around the axis perpendicular to the $(\tilde{r}, \theta)$ plane in $\{(0,0)\}$) and a Gaussian density on a circular domain, with different choices of the (adimensional) radius R: in particular, choosing $R = 4$, for $t \approx 0.44$ and $t \approx 0.60$ the density exhibits a zero in $\{(0,0)\}$ while the vorticity has there a maximum (see figures 8 and 10). For $t \approx 0.79$ again the density is zero in $\{(0,0)\}$ and suddenly the vorticity begins to increase too quickly, generating numerical errors (figure not reported). Concentration of the vorticity close to cylindrical sheets, often in correspondence with the minima or zeros of the density, is also observed during the whole simulation (analogous behaviours are observed for the other choices of R). As a last experiment, we perturb the harmonic potential by adding the term $C\tilde{\rho}$, $C > 0$: the behaviour is qualitatively the same as before, but concentration of vorticity close to the central lines is observed for slightly larger values of the energy.

The paper is organized as follows: in section 2 we recall the structure of the stationary solutions of the Schrödinger equation for bidimensional symmetric harmonic oscillator and some previous results concerning time-dependent Gaussian solutions for the new equations (1). The last are used to test the numerical scheme we introduce to numerically compute the non-Gaussian solutions of the system of PDEs (1). In section 3 we report our numerical results.

2. Stationary solutions and time-dependent Gaussian solutions for the symmetric bidimensional harmonic oscillator

2.1. Stationary solutions (analytical calculation)

Denoting by $(\tilde{x}, \tilde{y}, \tilde{z})$ the Cartesian coordinates in $\mathbb{R}^3$, we consider firstly *stationary solutions* of system (1) on the plane $(\tilde{x}, \tilde{y})$ with

$$\tilde{\Phi}(\tilde{r}) = \tfrac{1}{2} m\omega_{\mathrm{T}}^2 \tilde{r}^2, \qquad \tilde{r} = \sqrt{\tilde{x}^2 + \tilde{y}^2}.$$

It is convenient to introduce the *adimensional* variables

$$r = \frac{\tilde{r}}{a_{\mathrm{h}}}, \qquad t = \omega_{\mathrm{T}} \tilde{t}, \qquad \rho = a_{\mathrm{h}}^2 \tilde{\rho}, \qquad \boldsymbol{v} = \frac{\tilde{\boldsymbol{v}}}{a_{\mathrm{h}} \omega_{\mathrm{T}}}, \tag{5a}$$

where $a_{\mathrm{h}} = \sqrt{\hbar/2m\omega_{\mathrm{T}}}$, and

$$\begin{aligned} \boldsymbol{u}(\boldsymbol{x}, t) &= \nabla \ln \rho(\boldsymbol{x}, t) = \frac{\tilde{\boldsymbol{u}}(\tilde{\boldsymbol{x}}, \tilde{t})}{a_{\mathrm{h}} \omega_{\mathrm{T}}}, \\ \Phi(r) &= \frac{1}{2} r^2 = \frac{2\tilde{\Phi}(\tilde{r})}{\hbar \omega_{\mathrm{T}}}, \\ E(\rho, \boldsymbol{v}) &= \int_{\mathbb{R}^2} \left[\frac{1}{2} (|\boldsymbol{v}(\boldsymbol{x}, t)|^2 + |\boldsymbol{u}(\boldsymbol{x}, t)|^2) + \Phi(\boldsymbol{x}) \right] \rho(\boldsymbol{x}, t)\, \mathrm{d}\boldsymbol{x} = \frac{2\tilde{E}(\tilde{\rho}, \tilde{\boldsymbol{v}})}{\hbar \omega_{\mathrm{T}}}. \end{aligned} \tag{5b}$$

The energy derivative turns to be

$$\frac{\mathrm{d}}{\mathrm{d}t} E(\rho, \boldsymbol{v}) = -\int_{\mathbb{R}^2} |\nabla \wedge \boldsymbol{v}(\boldsymbol{x}, t)|^2 \rho(\boldsymbol{x}, t)\, \mathrm{d}\boldsymbol{x} = \frac{2}{\hbar \omega_{\mathrm{T}}^2} \frac{\mathrm{d}}{\mathrm{d}\tilde{t}} \tilde{E}(\tilde{\rho}, \tilde{t}); \tag{5c}$$

system (1) can be rewritten as

$$\begin{aligned} &\partial_t \boldsymbol{v} + (\boldsymbol{v} \cdot \nabla)\boldsymbol{v} - 2\nabla \left(\frac{\nabla^2 \sqrt{\rho}}{\sqrt{\rho}} \right) + (\nabla \ln \rho + \nabla) \wedge (\nabla \wedge \boldsymbol{v}) = -\nabla \Phi, \\ &\partial_t \rho = -\nabla \cdot (\rho \boldsymbol{v}) \end{aligned} \tag{6}$$

and the Schrödinger equation (2) becomes

$$\mathrm{i}\partial_t \psi = -\nabla^2 \psi + \tfrac{1}{2} \Phi \psi. \tag{7}$$

By the Energy Theorem all stationary solutions are irrotational almost everywhere. Therefore, we have to look for solutions of the corresponding Schrödinger equation of the type $\psi(r, \theta, t) = \chi(r, \theta) \exp(\mathrm{i}tE/2)$, with $\chi(r, \theta)$ and E denoting an eigenfunction and the corresponding eigenvalue of the quantum Hamiltonian, respectively. We consider then simultaneous eigenfunctions of the Hamiltonian and of the angular momentum with respect to the z-axis, which will be denoted by $\chi_{n_{\mathrm{d}}, n_{\mathrm{g}}}$, with $n_{\mathrm{d}}, n_{\mathrm{g}} = 0, 1, 2, \ldots$ The corresponding quantized energy is

$$E_{n_{\mathrm{d}}, n_{\mathrm{g}}} = 2(n_{\mathrm{d}} + n_{\mathrm{g}} + 1), \qquad n_{\mathrm{d}}, n_{\mathrm{g}} = 0, 1, 2, \ldots$$

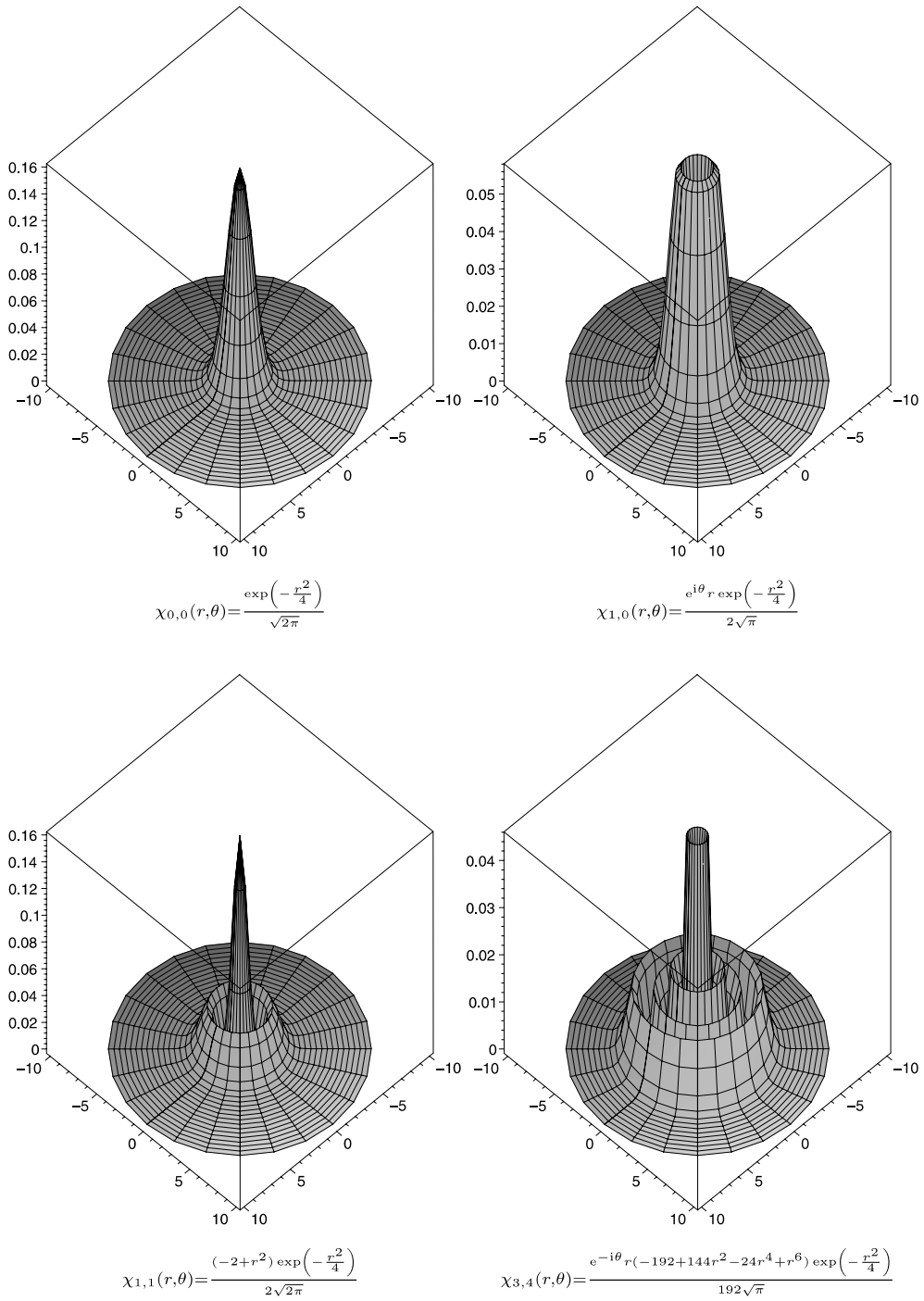

Figure 2. Plots of some $|\chi_{n_d,n_g}|^2$: systems of rings of zeros arise while increasing the energy.

The analytical expressions of χ_{n_d,n_g} can be calculated recursively starting from $\chi_{0,0}$ (cf [11]): we present in figure 2 some of their analytical expression as well as a 3D graphical representation of their square absolute value, computed by Maple®.

Thus, the stationary solutions of (6) with definite quantized angular momentum are of the type

$$\boldsymbol{v}_{n_\mathrm{d},n_\mathrm{g}}(r) = \frac{2\ell}{r}\hat{\theta}, \qquad \ell = n_\mathrm{d} - n_\mathrm{g}, \tag{8a}$$

$$\rho_{n_\mathrm{d},n_\mathrm{g}}(r) = |\chi_{n_\mathrm{d},n_\mathrm{g}}(r)|^2. \tag{8b}$$

For the sake of clarity, the dimensional expression of the velocity field, the density and the energy is given as

$$\begin{aligned}
\tilde{\boldsymbol{v}}_{n_\mathrm{d},n_\mathrm{g}}(\tilde{r}) &= \frac{\hbar\ell}{m\tilde{r}}\hat{\theta},\\
\tilde{\rho}_{n_\mathrm{d},n_\mathrm{g}}(\tilde{r}) &= \frac{2m\omega_\mathrm{T}}{\hbar}|\chi_{n_\mathrm{d},n_\mathrm{g}}(r)|^2,\\
\tilde{E}_{n_\mathrm{d},n_\mathrm{g}} &= (n_\mathrm{d} + n_\mathrm{g} + 1)\hbar\omega_\mathrm{T}.
\end{aligned} \tag{9}$$

Of course, these solutions are irrotational on $\mathbb{R}^2\backslash\{(0,0)\}$. Another class of solutions which could be handled analytically is that related to the oscillating Gaussian solutions of (2), for the harmonic potential: they are visualized, in particular, by the asymptotic trajectory in figure 3.

2.2. *Time-dependent Gaussian solutions (numerical computation for a system of ODEs)*

Let us now consider *initial data with non-zero vorticity*. The simplest smooth case is given by a linear velocity field and Gaussian symmetric density. We look for solutions of (6), which preserve the same properties. Therefore, the desired solutions are of the type

$$\boldsymbol{v}(r,t) = a(t)r\hat{r} - \Omega(t)r\hat{\theta} \quad (\text{from which } \nabla\wedge\boldsymbol{v}(t) = -2\Omega(t)), \tag{10a}$$

$$\rho(r,t) = \frac{A(t)}{2\pi}\exp\left[-\frac{A(t)}{2}r^2\right], \tag{10b}$$

where $A(t)$, $a(t)$ and $\Omega(t)$ are time-dependent scalar parameters with $A(t) > 0$ (cf [12]); we call them *linear-Gaussian solutions*. It can be easily seen that the time evolution of these solutions according to (6) is described by the first-order non-linear system of ODEs,

$$\begin{aligned}
\dot{A} &= -2aA,\\
\dot{a} &= A^2 + \Omega^2 - a^2 - 1,\\
\dot{\Omega} &= -2(a + A)\Omega.
\end{aligned} \tag{11}$$

In terms of (A, a, Ω), the energy functional and its time derivative become

$$E = \frac{1}{A}(A^2 + a^2 + \Omega^2 + 1), \qquad \frac{\mathrm{d}E}{\mathrm{d}t} = -4\Omega^2. \tag{12}$$

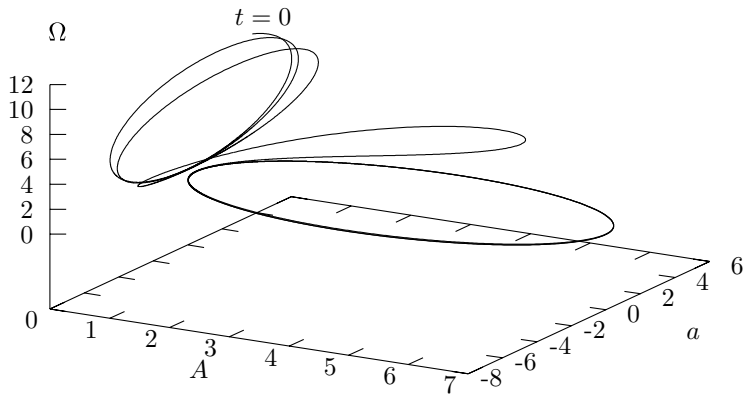

Figure 3. Trajectory of the solutions of system (11): the asymptotic orbit (with $\Omega = 0$) corresponds to a Gaussian oscillating solution of the Schrödinger equation.

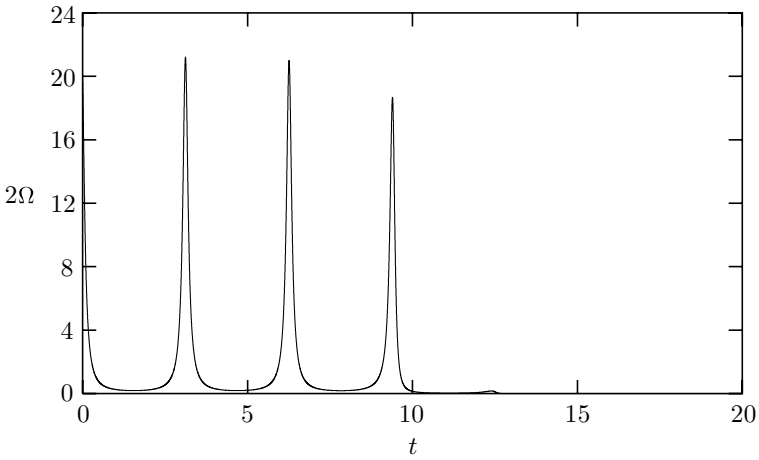

Figure 4. Time evolution of vorticity $-\nabla \wedge \boldsymbol{v} = 2\Omega$ in the time-dependent Gaussian case.

System (11) was studied by numerical methods in [12], where the global existence of the solutions and some stability results were also analytically proved. We revisit this work for the sake of clarity and because we will exploit linear-Gaussian solution to test the general numerical scheme. We have numerically integrated system (11) for the initial state $(A_0, a_0, \Omega_0) = (0.5, 2, 10)$ and $t \in [0, 20]$: the solution trajectory (A, a, Ω), the energy E and the vorticity Ω are plotted in figures 3–5.

2.3. Time-dependent Gaussian solutions by numerically solving the new system of PDEs and a numerical validation of the code

The next step is to numerically integrate system (6) on the bidimensional circular domain $D = B[0, R]$. Concerning the spatial discretization, we choose the FEM technique, with triangular finite elements, linear shape functions and standard Galerkin variational formulation, because it turns out to be quite simple to implement and more versatile (in the choice of the computational

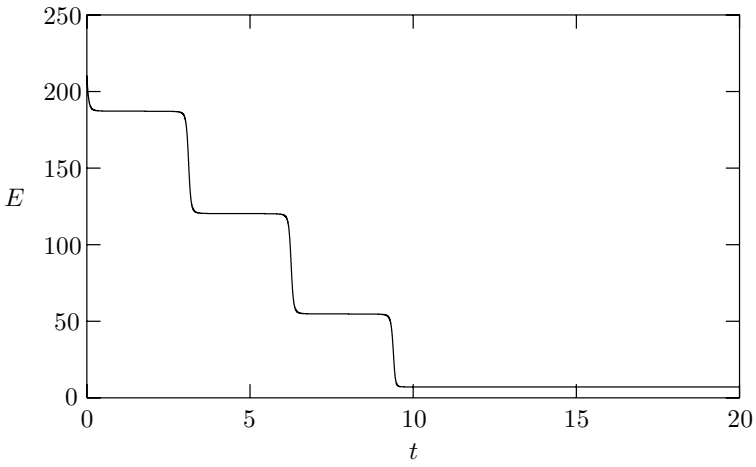

Figure 5. Time evolution of energy E in the time-dependent Gaussian case.

domain and possible mesh refinements) than other techniques, such as finite differences. Due to the linearity of shape functions, we have to reduce the system by one order: by introducing the (adimensional) osmotic velocity, the system can be rewritten as

$$\partial_t \boldsymbol{v} + (\boldsymbol{v}\cdot\nabla)\boldsymbol{v} - \nabla\left(\nabla\cdot\boldsymbol{u} + \tfrac{1}{2}\boldsymbol{u}\cdot\boldsymbol{u}\right) + (\boldsymbol{u}+\nabla)\wedge(\nabla\wedge\boldsymbol{v}) + \nabla\Phi = 0,$$
$$\partial_t \boldsymbol{u} + \nabla(\boldsymbol{u}\cdot\boldsymbol{v}) + \nabla(\nabla\cdot\boldsymbol{v}) = 0. \tag{13}$$

The continuity equation for ρ is also integrated to compute the energy E by (5b). The standard Galerkin variational formulation with linear basis functions we use is tailored to parabolic systems, whereas system (13) seems to have a hyperbolic form: using again the definition of the osmotic velocity we can write equivalently the system with a diffusive (and stabilizing) term in each equations. Concerning the time discretization, we adopt a ϑ-method which can be easily reduced to the implicit Euler scheme ($\vartheta = 1$) or to the Crank–Nicolson scheme ($\vartheta = \frac{1}{2}$), with adaptive time steps $\Delta t_k = t_{k+1} - t_k$. We use the Picard method for solving the non-linearity: even if linearly convergent, it is easily implementable, computationally cheaper and less sensible to the starting point than the classical (quadratically convergent) Newton–Raphson method.

First, we try to reproduce the linear-Gaussian solutions (10a), (10b) and (11), putting

$$\boldsymbol{v}_0(r) = a_0 r\hat{r} - \Omega_0 r\hat{\theta}$$

as initial current velocity field, a symmetric Gaussian function of the type

$$\rho_0(r) = \frac{A_0}{2\pi}\exp\left[-\frac{A_0}{2}r^2\right],$$

as initial density and the corresponding osmotic velocity field

$$\boldsymbol{u}_0(r) = \nabla \ln \rho_0(r).$$

The initial state (A_0, a_0, Ω_0) is the same as in the previous section, namely $(0.5, 2, 10)$. We have to impose appropriate boundary conditions on ∂D: since we are interested in a particular class of solutions, we force the boundary conditions of that class, which are known

in our case. In particular, at each time t_k, we solve the ODEs system (11) (as described in the previous section) with initial data $(A(t_k), a(t_k), \Omega(t_k))$ for a time step $\Delta t_k = t_{k+1} - t_k$ to obtain $(A(t_{k+1}), a(t_{k+1}), \Omega(t_{k+1}))$. This allows us to compute exactly the condition of the border for t_{k+1}. Then we solve system (13) with initial data $\rho(r, t_k)$, $\boldsymbol{u}(r, t_k)$ and $\boldsymbol{v}(r, t_k)$ and the known Dirichlet boundary conditions $\rho(R, t_{k+1})$, $\boldsymbol{u}(R, t_{k+1})$ and $\boldsymbol{v}(R, t_{k+1})$ for the same time step Δt_k. We observe that if we explore the evolution of the system for $t \in [0, T]$ with $T = 0.60$ (cf section 3 for the choice of T), it is sufficient, to get the *best* agreement allowed by the order of the numerical schemes, to choose, for example, the radius R of the domain equal to 4 and about 100 000 triangles for the mesh (we use triangle[4] to generate a mesh with 56 841 points and 113 090 triangles). For greater T one should increase R by keeping the same average area for the triangles.

3. Non-Gaussian solutions and concentration of vorticity close to central lines and cylindrical sheets

In this simulation, we choose, as initial data, the velocity field and the symmetric Gaussian density as in the previous test. We can note that, to obtain solutions different from the Gaussian ones, it is sufficient to impose different boundary conditions. From a physical point of view, the only necessary condition is $\rho = 0$ at infinity, while $\boldsymbol{u}$ and $\boldsymbol{v}$ are free (and in general strongly variable in time). However, integrating on a finite domain enforces the necessity of constraints of the boundary. In the next finite-element numerical experiments, the boundary conditions are

$$\begin{aligned} &-\nabla \cdot (\boldsymbol{u} - \boldsymbol{v})\Big|_{\partial D} \nu + \frac{\partial \boldsymbol{v}}{\partial \nu}\Big|_{\partial D} = 0, \\ &\boldsymbol{u}\Big|_{\partial D} = \boldsymbol{u}_0\Big|_{\partial D}, \\ &\rho\Big|_{\partial D} = \rho_0\Big|_{\partial D} \approx 0, \end{aligned} \tag{14}$$

where the first comes naturally from the finite-element discretization. We can notice that they are not satisfied by the linear-Gaussian solutions. This is sufficient to destroy the linearity. Notice also that some freedom is left to $\boldsymbol{v}$ and to the spatial derivatives of $\boldsymbol{u}$ and $\boldsymbol{v}$ on the border. In addition, since the density ρ must be zero at infinity and since ρ_0 is sufficient close to zero (for our numerical aims) on the boundary ∂D, we fix the values of ρ on ∂D at its initial values for the whole numerical simulation. The same for $\boldsymbol{u} = \nabla \ln \rho$. Putting conditions (14) at ∂D corresponds to introducing a perturbation of the scalar potential Φ at $r = R$. We stress again that the velocity field $\boldsymbol{v}$ and its derivatives are *not* fixed at ∂D. The initial conditions used, as just said, are

$$\begin{aligned} &\boldsymbol{v}_0(r) = a_0 r\hat{r} - \Omega_0 r\hat{\theta}, \quad a_0 = 2, \Omega_0 = 10, \\ &\boldsymbol{u}_0(r) = \nabla \ln \rho_0, \\ &\rho_0 = \frac{A_0}{2\pi} \exp\left(-\frac{A_0}{2} r^2\right), \quad A_0 = 0.5. \end{aligned}$$

[4] By J R Shewchuk, available at www.netlib.org/voronoi.

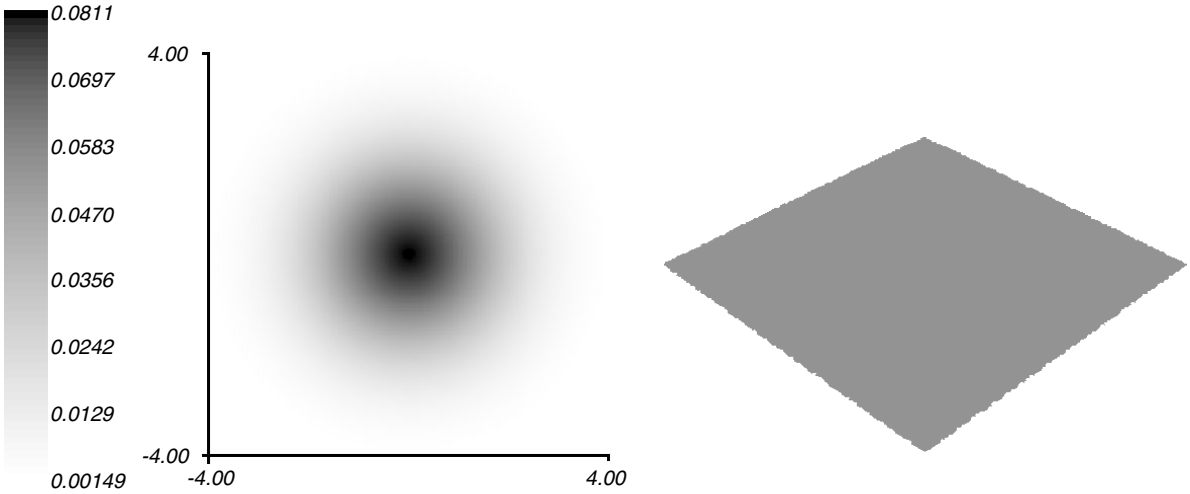

Figure 6. Density ρ and vorticity $-\nabla \wedge \boldsymbol{v}$ (zoom in $[-2, 2]^2$) at time $t = 0$, energy $E = 195$.

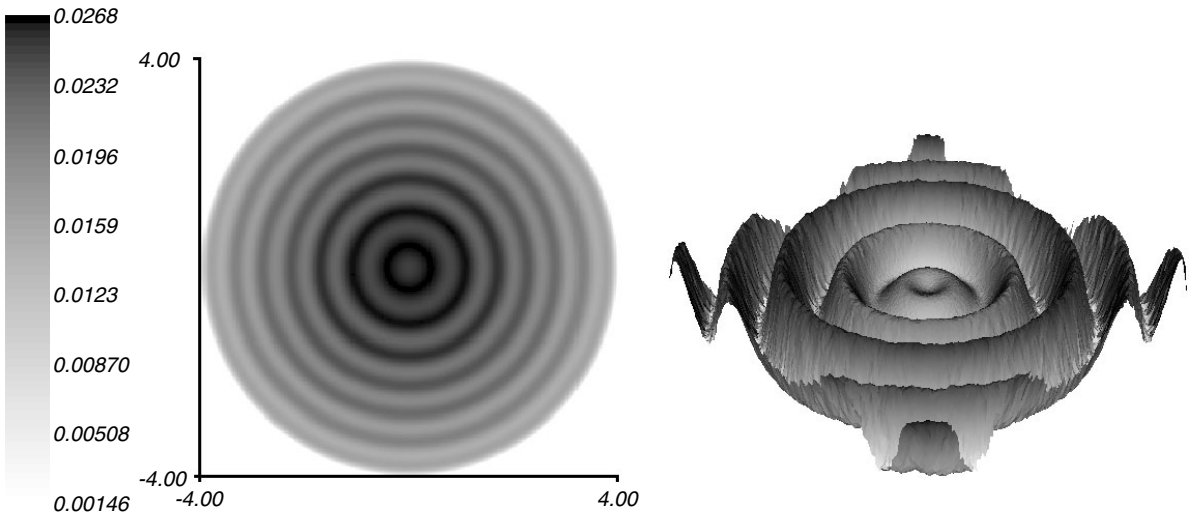

Figure 7. Density ρ and vorticity $-\nabla \wedge \boldsymbol{v}$ (zoom in $[-2, 2]^2$) at time $t = 0.25$, energy $E = 43$.

Since the time discretization of continuity equation can lead to a loss of the total mass, we renormalize to 1 the density at each time step before using (5b) to compute the energy.

In figures 6–10 we show the numerical computation of the density ρ and the vorticity $-\nabla \wedge \boldsymbol{v}$ at different times. We can observe that the vorticity does not monotonically decrease and tends to become concentrated close to cylindrical sheets and a central line (we suppose the system as being described in $\mathbb{R}^3$, the forces along the z-axis being equal to zero). In particular, in figures 8 and 10, a maximum of the vorticity in correspondence with a zero of the density takes place. For $t \approx 0.79$ again the density is zero in $\{(0, 0)\}$ and suddenly the

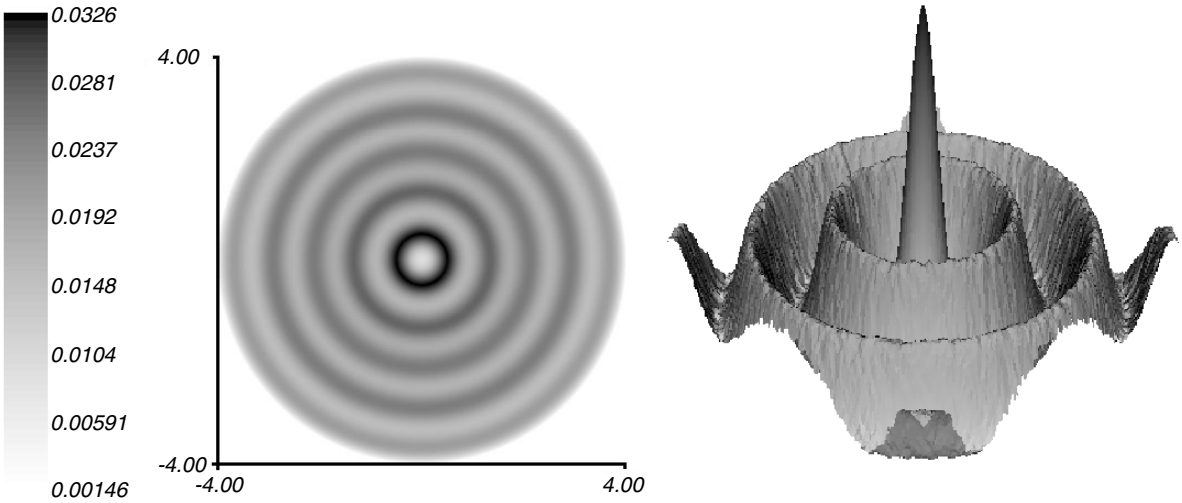

Figure 8. Density ρ and vorticity $-\nabla \wedge \boldsymbol{v}$ (zoom in $[-2, 2]^2$) at time $t = 0.44$, energy $E = 17$.

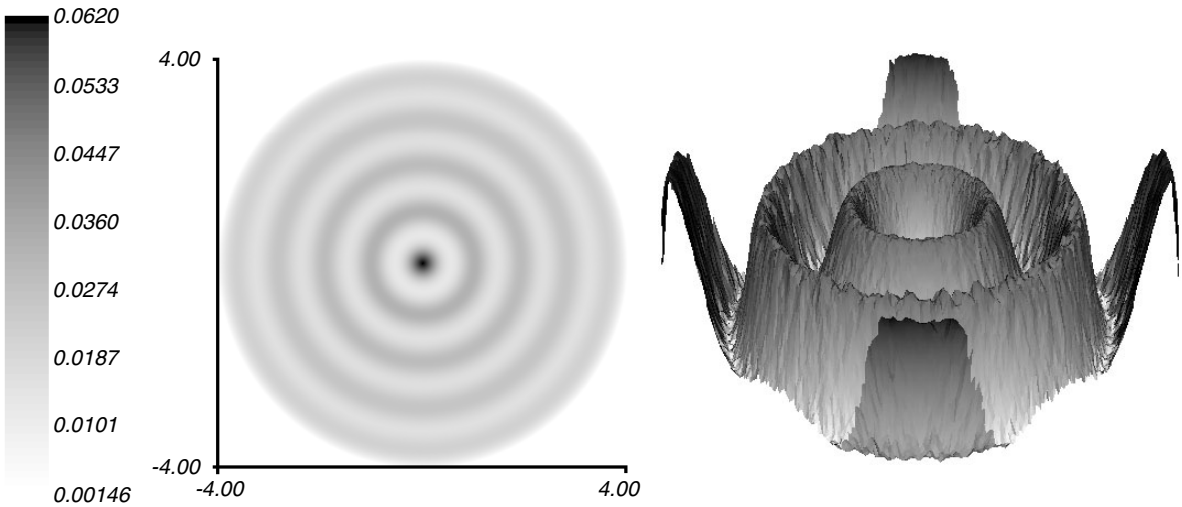

Figure 9. Density ρ and vorticity $-\nabla \wedge \boldsymbol{v}$ (zoom in $[-2, 2]^2$) at time $t = 0.50$, energy $E = 15$.

vorticity begins to increase too quickly, immediately generating numerical errors. It is quite difficult to get a good picture of what happens at this point (to give an idea, we report the final step of our experiment with $R = 10$ in figure 11). The evolution of energy is reported in figure 12. Notice that the energy numerically computed in this experiment is only a fraction of the total one, due to the size of the domain ($R = 4$) we have considered. To get an accurate approximation of the exact energy, one should take $R \geqslant 60$. Analogous simulations with different values of the radius R, as well as substituting $a_0 = 0$, exhibit the same qualitative behaviour.

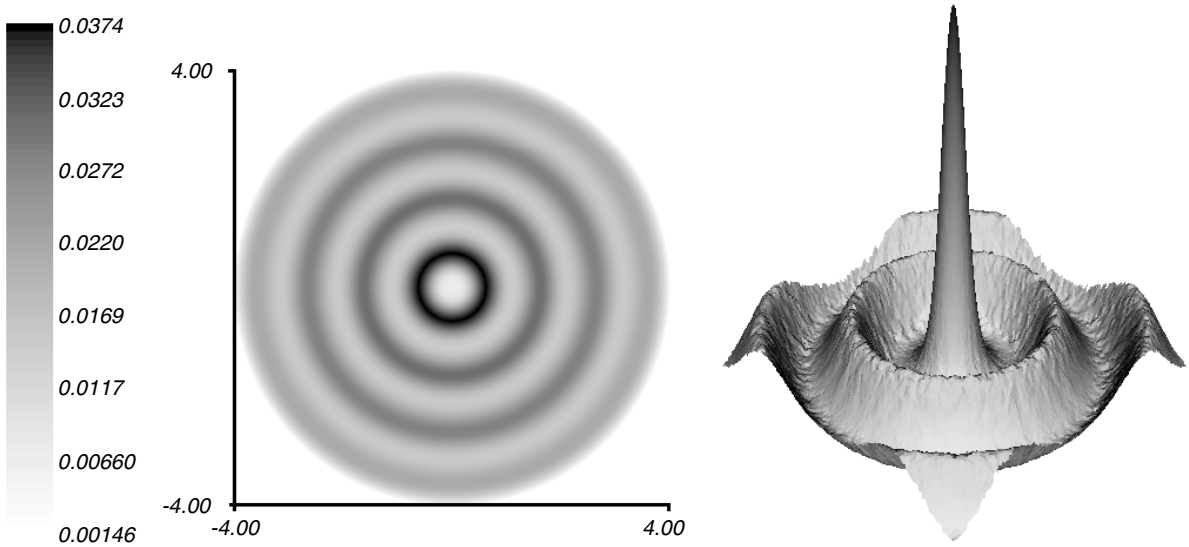

Figure 10. Density ρ and vorticity $-\nabla \wedge \boldsymbol{v}$ (zoom in $[-2, 2]^2$) at time $t = 0.60$, energy $E = 11$.

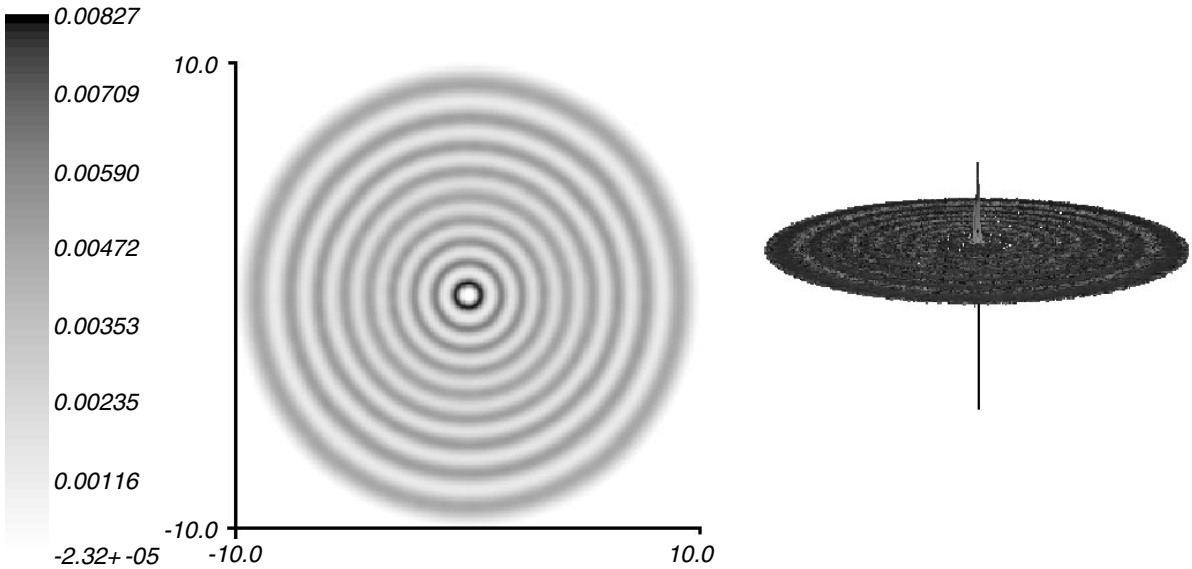

Figure 11. Density ρ and vorticity $-\nabla \wedge \boldsymbol{v}$ at the final step, $R = 10$.

As a last simulation, we repeat the previous test adding the Gross–Pitaevskii term to the harmonic potential:

$$\Phi(r, t) \to \Phi_{\mathrm{GP}}(r, t) = \tfrac{1}{2} r^2 + C\rho(r, t),$$

where C is an adimensional constant whose value was taken equal to 300 (cf [13]). The qualitative behaviour is the same as before, with the only difference that concentration of

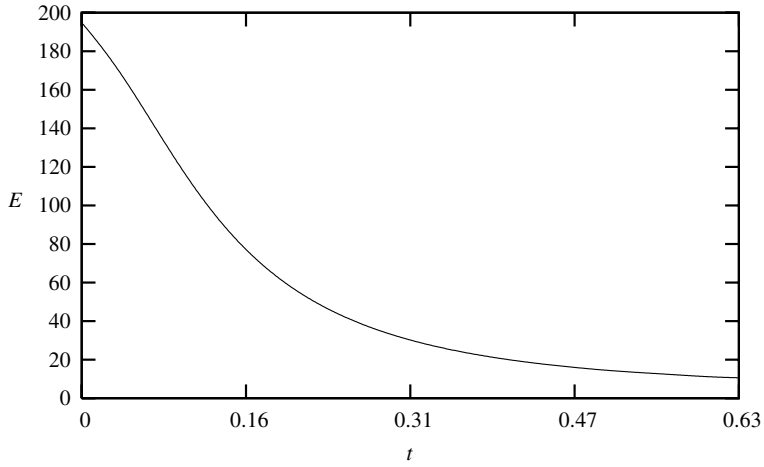

Figure 12. Time evolution of the energy E for symmetric initial data.

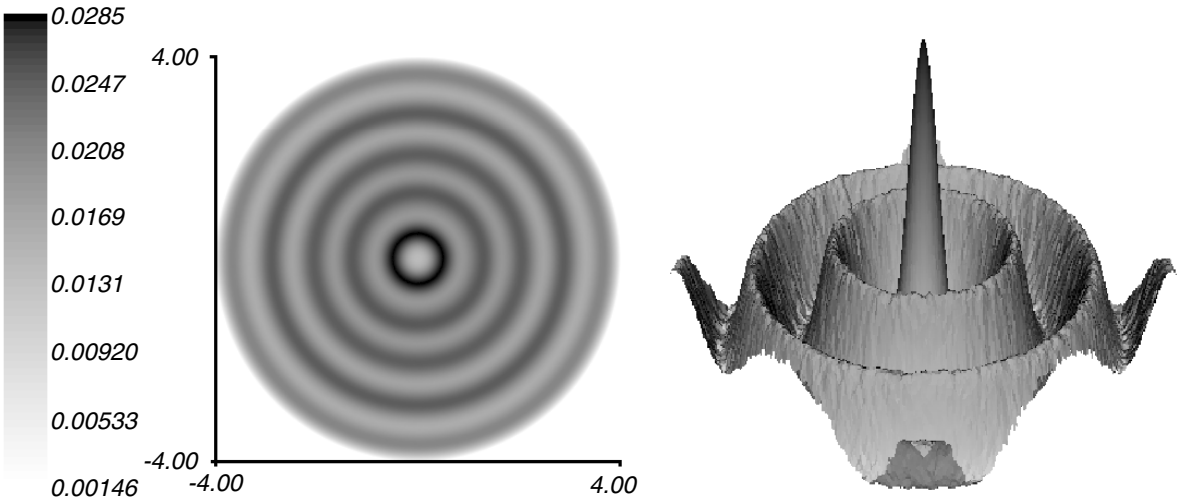

Figure 13. Density ρ and vorticity $-\nabla \wedge \boldsymbol{v}$ (zoom in $[-2, 2]^2$) at time $t = 0.44$, energy $E = 18$ (in the previous simulation $E = 17$), $\Phi \to \Phi_{\mathrm{GP}}$.

vorticity close to central lines is observed for slightly larger values of the energy (see figures 13–15).

4. Conclusions

Our numerical experiments confirm the conjecture that the generalization of Madelung equations given by (1) describes a dynamics which, starting from rotational initial data, asymptotically reproduces the quantum one, with the possibility of concentration of vorticity in the zeros of the density.

Such a phenomenon, at least in our example, does not seem to qualitatively change by adding the Gross–Pitaevskii term to the scalar potential.

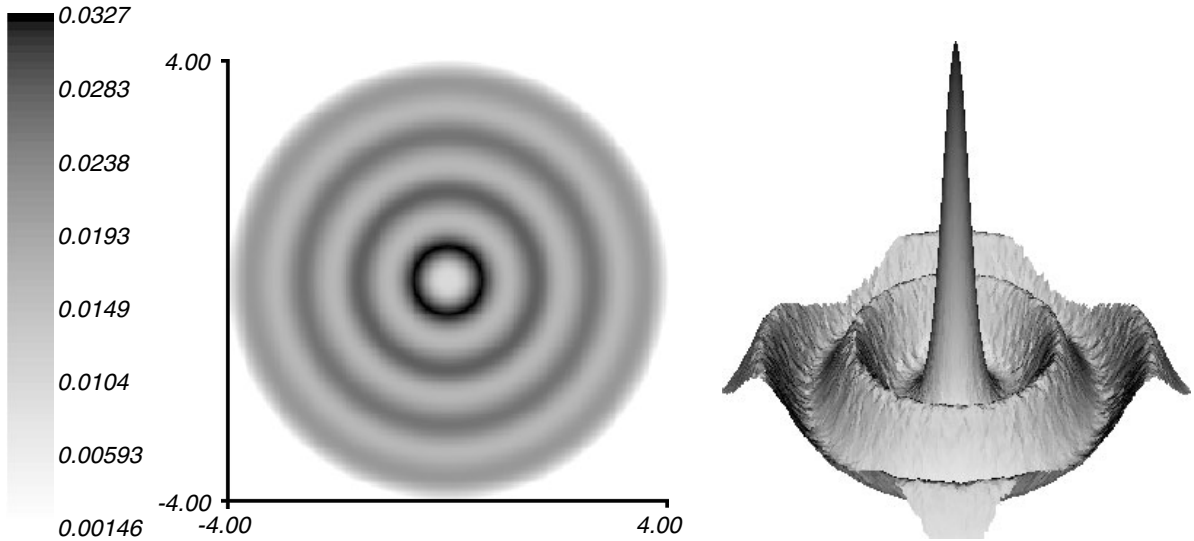

Figure 14. Density ρ and vorticity $-\nabla \wedge \boldsymbol{v}$ (zoom in $[-2, 2]^2$) at time $t = 0.60$, energy $E = 12$ (in the previous simulation $E = 11$), $\Phi \to \Phi_{\mathrm{GP}}$.

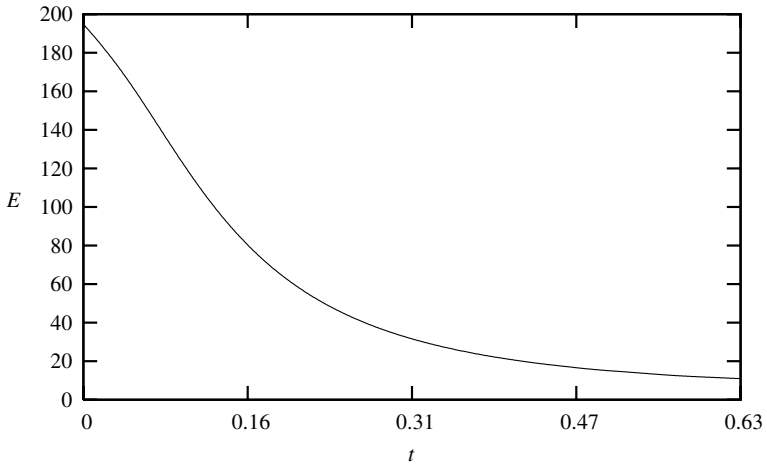

Figure 15. Time evolution of the energy E for symmetric initial data, $\Phi \to \Phi_{\mathrm{GP}}$.

It would be very interesting to study by means of analogous techniques the case with broken central symmetry or with a stirring potential, and compare the results, for example, with those obtained by Kasamatsu *et al* [13, 14].

Acknowledgments

LM is indebted to Professor Roberto Onofrio for his moral and scientific help. We also thank the numerical analysis group (in particular Professor Mario Putti) for their kind support at the Department of Mathematical Methods and Models for Applied Sciences of the University of Padova and Professor Roberto Giacobazzi at the Department of Computer Science of the University of Verona.

References

[1] Morato L M 1985 *Phys. Rev.* D **31** 1982
[2] Morato L M 1986 *Stochastic Processes in Classical and Quantum Systems (Ascona, 1985)* (*Lecture Notes in Physics* vol 262) ed S Albeverio, G Casati and D Merlini (Berlin: Springer) p 420
[3] Loffredo M and Morato L M 1989 *J. Math. Phys.* **30** 354
[4] Nelson E 1967 *Dynamical Theories of Brownian Motion* (Princeton, NJ: Princeton University Press)
[5] Nelson E 1985 *Quantum Fluctuations* (Princeton, NJ: Princeton University Press)
[6] Guerra F 1981 *Phys. Rep.* **77** 236
[7] Blanchard Ph, Combe Ph and Zheng W 1987 *Mathematical and Physical Aspects of Stochastic Mechanics* (*Lecture Notes in Physics* vol 281) (Berlin: Springer)
[8] Morato L M 1995 *Proc. Int. Conf. on Quantum-like Models and Coherent Effects (Erice, 1994)* ed R Fedele and P K Shukla (Singapore: World Scientific) p 97
[9] Aldovrandi E, Dohrn D and Guerra F 1992 *Acta Appl. Math.* **26** 219
[10] Guerra F 1988 *Ann. Inst. H. Poincaré Phys. Théor.* **49** 315
[11] Cohen-Tannoudji C, Diu B and Laloe F 1978 *Quantum Mechanics* (New York: Wiley)
[12] Morato L M and Ugolini S 1994 *Ann. Inst. H. Poincaré Phys. Théor.* **60** 323
[13] Kasamatsu K, Tsubota M and Ueda M 2003 *Phys. Rev.* A **67** 033610
[14] Tsubota M, Kasamatsu K and Ueda M 2002 *Phys. Rev.* A **65** 023603